HHS Public Access

Author manuscript

Science. Author manuscript; available in PMC 2023 February 11.

Published in final edited form as:

Science. 2022 February 11; 375(6581): eabi5965. doi:10.1126/science.abi5965.

CD97 promotes spleen dendritic cell homeostasis through the mechanosensing of red blood cells

Dan Liu[1,2], **Lihui Duan**[1,2], **Lauren B Rodda**[1,2,#], **Erick Lu**[1,2,†], **Ying Xu**[1,2], **Jinping An**[1,2], **Longhui Qiu**[3], **Fengchun Liu**[3], **Mark R Looney**[3], **Zhiyong Yang**[4,5,6,‡], **Christopher D C Allen**[4,5,6], **Zhongmei Li**[7], **Alexander Marson**[2,3,7], **Jason G Cyster**[1,2,*]

[1]Howard Hughes Medical Institute, University of California San Francisco, San Francisco, CA 94143, USA.

[2]Department of Microbiology and Immunology, University of California San Francisco, San Francisco, CA 94143, USA.

[3]Department of Medicine, University of California San Francisco, San Francisco, CA 94143, USA.

[4]Cardiovascular Research Institute, University of California San Francisco, San Francisco, CA 94143, USA.

[5]Sandler Asthma Basic Research Center, University of California San Francisco, San Francisco, CA 94143, USA.

[6]Department of Anatomy, University of California San Francisco, San Francisco, CA 94143, USA.

[7]J. David Gladstone Institutes, San Francisco, CA 94158, USA.

Abstract

Dendritic cells (DCs) are crucial for initiating adaptive immune responses. However, the factors that control DC positioning and homeostasis are incompletely understood. Here we found that type-2 conventional DCs (cDC2s) in the spleen depend on $G\alpha_{13}$ and adhesion G protein-coupled receptor family member-E5 (Adgre5, or CD97) for positioning in blood-exposed locations. CD97 function required its autoproteolytic cleavage. CD55 is a CD97 ligand and cDC2 interaction with CD55-expressing red blood cells (RBCs) under shear stress conditions caused extraction

*Corresponding author. Jason.Cyster@ucsf.edu.

Author contributions: D.L. and J.G.C. conceived the project, designed the experiments, interpreted the results, and wrote the manuscript. D.L. conducted the experiments. L.D. analyzed the RNAseq data. L.B.R. made initial observations in ArhGEF1-deficient mice. E.L. performed RNAseq of ArhGEF1-deficient cDC2s. Y.X. performed molecular biology experiments. J.A. genotyped mice. L.Q. and M.R.L. performed spleen transplantation and IVC ligation from the UCSF microsurgery core. F.L. and M.R.L. performed surgery to collect blood from splenic artery and vein. Z.Y. and C.D.C.A. provided the pQEF vector. Z.L., Y.X. and A.M. generated the CD97-deleted and CD55-deleted mouse lines.

#Current address: Department of Immunology, University of Washington School of Medicine, Seattle, WA 98109, USA.
†Current address: Gilead Sciences, Foster City, CA 94404, USA.
‡Current address: Department of Immunology Discovery, Genentech, South San Francisco, CA 94080, USA.

Competing interests: J.G.C. is an advisor for MiroBio and Be Biopharma and owns stock in ALX Oncology. A.M. is a compensated cofounder, member of the boards of directors, and a member of the scientific advisory boards of Spotlight Therapeutics and Arsenal Biosciences. A.M. owns stock in Arsenal Biosciences, Spotlight Therapeutics, Merck and PACT Pharma; A.M. is an investor in and informal advisor to Offline Ventures..

Data and materials availability: GSE77671 was used to compare CD97-regulated genes in mice with splenic human dendritic cells. Raw RNA-seq data have been deposited at GEO, accession no. is GSE188835. All other data are available in the main text or the supplementary materials.

of the regulatory CD97 N-terminal fragment. Deficiency in CD55-CD97 signaling led to loss of splenic cDC2s into the circulation and defective lymphocyte responses to blood-borne antigens. Thus, CD97 mechanosensing of RBCs establishes a migration and gene expression program that optimizes the antigen capture and presentation functions of splenic cDC2s.

Sentinel conventional dendritic cells (cDCs) are stationed in most tissues of the body, where they continually sample their microenvironment for antigens (1, 2). The spleen is a large lymphoid organ involved in surveying the blood for pathogens and clearing defective red blood cells (RBCs) (3). The spleen is unusual in having an open circulation, in which terminal arterioles release blood into the marginal zone (MZ) that surrounds the lymphocyte-rich white pulp, or directly in to the macrophage-rich red pulp (4, 5). Two main classes of cDCs are present in the spleen: cDC1s and cDC2s (1, 2). By promoting CD4 T cell activation and T follicular helper (T_{FH}) cell generation, cDC2s are important for B cell responses. Many splenic cDC2s are positioned in regions of the spleen that connect the T cell-zone with the red pulp, which are known as MZ bridging channels. Cells in the outer parts of the bridging channel, the MZ, and the red pulp are directly exposed to blood flow, and this facilitates their encounter with circulating antigens (6-10). cDC2s depend on the chemoattractant receptor EBI2 (GPR183) to position in MZ bridging channels (6, 11), and these cDCs are also dependent on IRF4, Notch, and integrins for their homeostasis (1, 2). However, the mechanisms that allow cDC2 exposure to blood flow while ensuring their retention in the spleen are poorly understood. We define a critical role for an adhesion G protein-coupled receptor (GPCR) in sensing passing blood cells and promoting splenic cDC2 homeostasis and function.

Results

Splenic cDC2s depend on $G\alpha_{13}$ signaling

Because $G\alpha_{13}$-coupled receptors can promote confinement of cells within tissue compartments (12, 13), we asked whether the $G\alpha_{13}$-signaling pathway was required for cDC positioning. The Rho guanidine nucleotide exchange factor (GEF) ArhGEF1 is an effector of $G\alpha_{13}$-containing heterotrimeric G-proteins (12). We observed by means of flow cytometry and immunofluorescence microscopy that ArhGEF1-deficient mice suffered a splenic cDC2 deficiency (Fig. 1, A to C, and fig. S1, A and B). cDC2s were identified by use of DCIR2 because this marker stains the majority of splenic cDC2s (fig. S1A) and allows their selective staining in tissue sections. Similar reductions in cDC2s were observed when other markers were used (fig. S1B). Splenic cDC1 frequencies were not significantly affected by ArhGEF1 defciency (Fig. 1A and fig. S1C). Mixed bone marrow (BM) chimera experiments established that the splenic cDC2 deficiency reflected a cell-intrinsic role for ArhGEF1 (Fig. 1D to F). Under these competitive conditions, a reduction in cDC1s was also observed (Fig. 1D and fig. S1D). We next determined whether $G\alpha_{13}$ was required for splenic cDC homeostasis. *Gna13*$^{f/f}$ *CD11c*-Cre mice (referred to as *Gna13*^{cKO}) had a selective cDC2 deficiency similar to *Arhgef1*$^{-/-}$ mice (Fig. 1, A to C, and fig. S1, C and E). Deficiency in the gene encoding the related Gα12 protein had no effect on cDC frequencies (fig. S1F and G). Mice lacking both $G\alpha_{13}$ and ArhGEF1 had the same extent of splenic

cDC2 deficiency as that of the single mutants, which is consistent with these molecules acting in the same pathway (Fig. 1, A to C).

Examining the basis for the reduced cDC2 frequencies, we performed intravascular labeling to measure whether cDC2s were not properly positioned in blood-exposed locations (7-9). We used mixed BM chimeras to allow comparison of wild-type (WT) and $G\alpha_{13}$-deficient cells in the same mice. These mice showed a reduction in *Gna13*^{cKO} cDC2s, whereas the cDC1 compartment remained intact (Fig. 1G and fig. S1H). *Gna13*^{cKO} cDC2s remaining in the spleen were less strongly labeled by intravascular antibody (Fig. 1, H and I). By contrast, $G\alpha_{13}$ deficiency did not alter the labeling of cDC1s (fig. S1I). A possible explanation for the reduced labeling of cDC2s was the loss of mutant cells into the bloodstream. We detected an increased frequency of cDC2s in blood circulation of ArhGEF1- and $G\alpha_{13}$-deficient mice (Fig. 1J). Once in blood circulation, cDC2s are rapidly lost, most likely through their capture and clearance by phagocytic cells (9). Investigating other possible causes for the reduction in cDC2s, there was no significant alteration in the frequency of pre-DCs in BM and spleen of *Arhgef1*$^{-/-}$ or *Gna13*^{cKO} mice (fig. S1, J and K). Among the splenic cDC2s remaining in *Gna13*^{cKO} mice, a greater fraction were actively dividing (fig. S1L). Apoptotic cell frequencies were low in control mice and were similar in *Gna13*^{cKO} mice (fig. S1M). Expression of the Notch2-induced surface molecule, ESAM (14), was not altered on the cDC2s remaining in $G\alpha_{13}$- and ArhGEF1-deficient mice, which suggests that Notch2 signaling was intact (fig. S1N). Thus, the reduced cDC2 frequencies in spleens of ArhGEF1- and $G\alpha_{13}$-deficient mice appear to be a consequence of cDC2 loss into blood circulation.

CD97 functions upstream of $G\alpha_{13}$

The $G\alpha_{13}$ requirement for splenic cDC2 homeostasis implicated involvement of a GPCR. To search for such a receptor, we used an in vivo CRISPR-based mutagenesis screen of 20 GPCRs abundantly expressed by cDC2s. Only a mutation of the adhesion GPCR family member E5 (Adgre5, also known as CD97) led to a reduction in cDC2s (Fig. 2, A and B). Typical of adhesion GPCRs, CD97 has an extended N-terminal extracellular domain (15-17) (Fig. 2C). This region of CD97 is alternatively spliced and includes three or four epidermal growth factor (EGF) domains and a GPCR autoproteolysis-inducing (GAIN) domain that contains the GPCR proteolysis site (GPS). The N-terminal fragment (NTF) of CD97 remains non-covalently bound to the seven-transmembrane part of the receptor after autoproteolytic cleavage (15, 18). CD97 binds several ligands in vitro including CD55, chondroitin sulfate, Thy1, and integrins $\alpha_5\beta_1$ and $\alpha_v\beta3$ (15, 19). An antibody against CD97 blocks some of these interactions (20). Treatment with this antibody led to a selective reduction in the splenic cDC2 frequency (Fig. 2D and fig. S2A).

We generated mice lacking CD97 (fig. S2, B and C) and confirmed that CD97 was required for splenic cDC2 but not cDC1 homeostasis (Fig. 2, E and F and fig. S2, D and E). Peripheral lymph node (pLN) cDC homeostasis was unaffected (fig. S2, F and G) and BM and splenic pre-DC frequencies were normal (fig. S2H). Mixed BM chimera experiments confirmed the intrinsic requirement for CD97 in cDC2s (Fig. 2G) but not cDC1s (fig. S2, I and J). Intravascular labeling in BM chimeras showed that the CD97-deleted cDC2s remaining in the spleen had reduced blood exposure compared to the WT cDC2s in the same

animals (Fig. 2H). Mice in which CD97 was deleted had increased frequencies of cDC2s in blood circulation (fig. S2, K and L). Sampling of blood in the splenic artery and vein revealed that cDC2s were most increased in the vein in accord with cell loss from the spleen and rapid clearance from circulation (Fig. 2I). Splenic cDC2s endogenously expressed long and short CD97 isoforms (fig. S2M). Using retroviral transduction experiments, the full-length isoform and the short isoform that contains EGF domains 1, 2, and 4 could rescue the cDC2 deficiency in mice in which CD97 was deleted (Fig. 2J and fig. S2N). A CD97 mutant lacking a C-terminal PDZ-binding motif (PBM) (21) retained function (Fig. 2J). In vitro studies have suggested that autoproteolytic cleavage of the NTF from the GPCR domain is important for receptor function (21-23). Changing a conserved Thr (T) residue at the +1 position of the CD97 GPS to Gly (G) disrupts autoproteolysis (21). This T419G mutant of CD97 was unable to rescue cDC2 frequencies in mice in which CD97 was deleted, despite being well expressed (Fig. 2J). Thus, autoproteolysis is necessary for in vivo CD97 function in cDC2s.

Further approaches were used to test whether CD97 was acting in the same pathway as $G\alpha_{13}$, and ArhGEF1. Mutation of CD97 in ArhGEF1-deficient mice did not have any effect, which is consistent with CD97 functioning upstream of $G\alpha_{13}$ and ArhGEF1 (Fig. 2K). cDC2s from ArhGEF1-, $G\alpha_{13}$-, and CD97-deficient mice had highly similar gene expression profiles, further indicating that these molecules are in a common pathway (fig. S3, A to D). This analysis revealed lower expression of F4/80 (Emr1 or Adgre1) in the mutant cDC2s, which was confirmed by flow cytometry (fig. S3E). Analysis of available human spleen cDC gene expression data (24) showed high expression of CD97 by $CD1c^+$ cDC2s (fig. S3F). Gene set enrichment analysis (GSEA) revealed that human splenic cDC2s were enriched for CD97 pathway dependent genes compared to $CD141^+$ cDC1s and were depleted for genes that were upregulated in CD97-deficient cells (fig. S3G). Thus, the CD97-pathway dependence of splenic cDC2s is most likely conserved in humans.

CD55-expressing RBCs activate CD97 on splenic cDC2s

CD55, the decay accelerating factor (DAF) of complement, binds the first two EGF domains of CD97. Treatment of mice with an antibody to CD55 (15) that blocks this binding led to a selective decrease in splenic cDC2 frequencies (Fig. 3A and fig. S4A) and the appearance of cDC2s in blood circulation (Fig. 3B). We generated mice in which CD55 was deleted (fig. S4, B and C) and found reduced frequencies of splenic cDC2s (Fig. 3C and fig. S4D). The frequencies of splenic cDC1s (Fig. S4E), pLN cDCs (fig. S4F), and BM and spleen pre-DCs were not altered (fig. S4G). Like the other mutant strains, CD55-deficient mice had increased cDC2s in blood (Fig. 3D and fig. S4H). CD55 is widely expressed by hematopoietic and non-hematopoietic cells (15, 19), although it is not expressed by splenic DCs (Fig. 3E and fig. S4I). Staining of spleen sections showed broad CD55 expression, including on endothelial and stromal cells (fig. S4J). However, BM chimera experiments established that CD55 expression by hematopoietic cells and not by radio-resistant stromal cells was needed for cDC2 homeostasis (Fig. 3F). Despite the strong CD55 expression by B cells (Fig. 3E and fig. S4I), when B cells or T cells or all lymphocytes lacked CD55, cDC2 homeostasis remained intact (Fig. 3, G to I, and fig. S4, K and L).

RBCs also strongly express CD55 (19) (Fig. 3J). Since the most prominent loss of cDC2s in the mutant strains is that of blood-exposed cells and given that RBCs constitute ~99.9% of circulating cells (25), we asked whether RBCs could be a sufficient source of CD55 to maintain cDC2 homeostasis. Transfer of purified WT RBCs to hosts in which CD55 was deleted, so that they constituted one-third of the circulating RBCs (Fig. 3K and fig. S4M), was sufficient to substantially restore cDC2 homeostasis (Fig. 3, L and M and fig. S4N). Transfers of white blood cells (WBCs) did not restore the cDC2 compartment (fig. S4O). Platelets were present in mouse blood at about 5% the frequency of RBCs and also expressed CD55 (fig. S4, P and Q). Mice genetically deficient in platelets or lacking CD55 on platelets maintained a normal splenic cDC2 compartment, however (Fig. 3N and fig. S4, P to S). Thus, RBCs are the dominant source of CD55 needed for splenic cDC2 homeostasis.

Surface levels of CD97 on spleen and blood lymphocytes are elevated in mice lacking CD55 (26) (fig. S5, A and B). Modulation of CD97 on lymphocytes is suggested to depend on engagement by CD55 under conditions of shear stress, with the NTF likely being extracted by pulling forces (26). Because the antibody used to detect CD97 is NTF-specific, it provides a measure of the intact heterodimeric form of CD97 (Fig. 2C). When the NTF separates away from the heterodimer, the membrane-associated GPCR domain can no longer be detected. NTF^+ CD97 abundance on splenic cDC2s was elevated in mice in which CD55 was deleted (Fig. 4A). In the CD55-deficient mice reconstituted with WT RBCs, NTF^+ CD97 abundance on cDC2s was reduced (Fig. 4A). Using another approach, we examined the effect of short-term blockade of the CD55–CD97 interaction. In experiments where mice were treated with the CD55 blocking antibody, NTF^+ CD97 became more strongly elevated on blood-exposed splenic cDC2s (Fig. 4B and fig. S5C). In mice expressing the T419G noncleavable mutant of CD97, blocking CD55 had no effect on CD97 levels on blood-exposed cDC2s (Fig. 4C and fig. S5D). We then tested the impact of stopping blood flow through the inferior vena cava (IVC) by tying off the vessel for 30 min (movie S1). These mice were injected intravenously with splenocytes immediately before the vessel ligation. Transferred cDC2s and B cells in the region with flow (heart) had reduced NTF^+ CD97 compared with those in the IVC, where flow was stopped (Fig. 4D and fig. S5E). When the same experiment was performed in CD55-deficient mice, there was no difference in NTF^+ CD97 on cDC2s and B cells in regions with or without blood flow (Fig. 4D and fig. S5E). Thus, cDC2s interacting with RBCs in vivo under conditions of shear stress undergo CD55-mediated extraction of the CD97 NTF.

To more directly test whether the CD97 NTF on cDC2s was extracted upon interaction with $CD55^+$ RBCs under shear stress conditions, we incubated spleen cells with WT or CD55-deleted RBCs. In the absence of shear stress, cDC2s maintained abundant cell-surface NTF^+ CD97. However, under shear stress conditions, NTF^+ CD97 expression by cDC2s was significantly reduced (Fig. 4E). When the added RBCs lacked CD55, shear stress conditions did not lead to any modulation of NTF^+ CD97 (Fig. 4E). The reduction in surface NTF^+ CD97 was matched by a reduction in total NTF^+ CD97, suggesting that the reduced surface levels were not due to CD97 internalization (fig. S5, F and G). When cDC2s expressing the T419G ectodomain cleavage-resistant CD97 mutant were exposed to WT RBCs under shear stress conditions, there was no change in surface NTF^+ CD97 (Fig. 4F). Last, we studied

cDC2s expressing CD97 with green fluorescent protein (GFP) fused at the C-terminus. Incubation with RBCs under shear stress conditions led to reduced NTF$^+$ CD97 but did not alter abundance of the CD97 GPCR domain as reported by GFP intensity (fig. S5, H and I). Thus, cDC2 exposure to RBCs under shear stress conditions is sufficient to lead to extraction of the CD97 NTF without changing the abundance of the GPCR domain.

CD97 pathway restrains F-actin and actin-regulated transcription

Because Rho is a major regulator of cytoskeletal dynamics, we stained cells from the gene-deficient mouse lines for F-actin content. In every case, cDC2s from mutant mice had increased F-actin compared with that of cDC2s from WT mice (Fig. 5, A and B, and fig. S6, A and B). Blocking antibody treatment also led to an increase in F-actin content on blood-exposed cDC2s (Fig. 5, C and D). Analysis of splenic cDC1s showed a slight increase in F-actin content in *Arhgef1*$^{-/-}$ but not *Gna13*^{cKO}, *Adrge5*$^{-/-}$ or *Cd55*$^{-/-}$ mice (fig. S6, C to F). Mrtf-a is a transcription factor that is kept in an inactive and predominantly cytoplasmic form by binding to G-actin. When G-actin is consumed to form F-actin, Mrtf-a accumulates in the nucleus as an active transcription factor (27, 28). GSEA showed that Mrtf-a-dependent genes (29) were upregulated in ArhGEF1- and CD97-deficient cDC2s (Fig. 5E). Many of the Mrtf-a-regulated genes encode for cytoskeletal proteins (27, 28), and several such genes were upregulated in CD97-deficient cDC2s (fig. 5F). Hematopoietic cells lacking Mrtf-a (and the related gene, Mrtf-b) show poor migratory responses (29, 30). Thus, Mrtf-induced gene expression may contribute to altered motility of cDC2s deficient in the CD97 pathway.

CD97 pathway restrains splenic cDC2 migration

We next used intravital microscopy to observe splenic cDC migration. We intercrossed *Batf3*$^{-/-}$ mice that lack cDC1s (31) (fig. S6, G and H) with CD11c-YFP (yellow fluorescent protein) reporter mice and *Arhgef1*$^{-/-}$ mice. Analysis of tissue sections showed that the majority of CD11c-YFP$^+$ cells in these mice were DCIR2$^+$ cDC2s, and their density was reduced in mice lacking ArhGEF1 (fig. S6G). Real-time intravital imaging revealed that although most cDC2s showed little migratory activity, occasional cells were detected that were actively migratory (Fig. 5G and movie S2). Rare cells could also be detected moving into large blood vessels (likely red pulp sinuses), in some cases through active migration (Fig. 5G and movie S3). In other cases, cells appeared to already be detached, rounded up, and in flow within the red pulp at the time of reaching a large vessel (movie S4). Like intravascular DCs in dermal lymphatics (32), intravascular cDC2s often continued to migrate for a period of time before being carried away into the blood flow (Fig. 5G and movies S3 and S4). Despite the overall reduction in cDC2s detectable per frame (fig. S6I), there was an increased frequency of migratory cDC2s in ArhGEF1-deficient mice (Fig. 5H and movies S5 to S8). Moreover, an increased frequency of cDC2s was observed moving into large blood vessels and being caught in flow (Fig. 5I and movies S5 to S8). In accord with the imaging data, there was an increased frequency of ArhGEF1-deficient CD11c-YFP$^+$ cDC2s in the blood circulation (Fig. 5J).

As another approach to test for cDC2 movement from the spleen into the blood, we transplanted spleens from *Gna13*^{cKO} or control mixed chimeric mice into WT recipients. Eight to nine hours after the surgery, we examined the recipient blood for donor-derived B

cells and cDC2s. The frequency of B cells in the blood closely matched the chimerism in the transplanted spleen, whereas cDC2s in blood were signficiantly enriched for *Gna13*^{cKO} cDC2s (Fig. 5, K to N and fig. S6J). Thus, $G\alpha_{13}$-deficient cDC2s have altered migratory behavior that results in their loss from the spleen into the blood circulation.

Deficiency in the CD97 pathway alters DC function

To test the impact of deficiency in the CD97 pathway on DC activation and function, we immunized mice with a model systemic antigen, sheep red blood cells (SRBCs). Three hours after immunization, there was a selective defect in antigen acquisition by the CD97-deficient cDC2s (Fig. 6A and fig. S7A). In accord with the reduced antigen capture, CD97-deleted cDC2s showed less efficient activation as assessed by CCR7 and CD86 up-regulation (Fig. 6B and fig. S7B). Similar SRBC-induced cDC2 activation defects were observed in ArhGEF1-deficient mice (fig. S7, C to E). Moreover, CD4 T cell proliferation in response to SRBC-associated antigen was reduced in CD97-deleted compared with WT recipients (fig. S7, F and G). To exclude possible roles for the CD97–$G\alpha_{13}$ pathway in other cell types, we performed the same experiment in mice lacking $G\alpha_{13}$ selectively in CD11c^{+} cells and again observed defective T cell proliferation (Fig. 6, C and D). The responding T cells up-regulated ICOS and PD1 to a lesser degree, suggesting reduced induction of T_{FH} cells (Fig. 6E and fig. S7, H and I). Both *Gna13*^{cKO} and CD97-deleted recipient mice also showed a reduced germinal center (GC) response to SRBC-associated antigen (Fig. 6F and fig. S7, J and K). cDC2s have been implicated in the splenic B cell response to heat-killed *Listeria monocytogenes* (HKLM) (33). After immunization with HKLM, CD97-deficient mice mounted a reduced GC response (Fig. 6G). RBC alloimmunization can induce hemolytic transfusion reactions, potentially resulting in hemolytic diseases and renal failure (7, 34). Using transfers of foreign antigen conjugated mouse RBCs to model RBC allotranfusion, DC $G\alpha_{13}$ deficiency resulted in a reduced allo-RBC antibody response (Fig. 6H).

To determine whether the reduced splenic DC function in CD97 pathway-deficient mice could be explained by the reduced cDC2 frequency or also reflected defects in the function of the remaining cDC2s, we used a BM chimeric approach to generate mice that contained matched frequencies of WT or CD97-deleted cDC2s (fig. S8, A and B). When these mice were immunized with SRBC-associated antigen, control and CD97-deficient chimeric mice showed similarly reduced T cell responses compared to mice with a normally sized cDC2 compartment (fig. S8C). Thus, the reduced cDC2 compartment size appears to be a key contributor to the reduced T cell response in mice lacking the CD97 pathway. Antigen capture capability of WT cDC2s remained intact in mice with a low cDC compartment size (fig. S8D). However, CCR7 up-regulation on WT cDC2s in these mice was impaired (fig. S8, E and F). Thus, CD97-mediated maintenance of a normally sized cDC2 compartment is necessary for cDC2 function. Moreover, when cDC2 numbers drop, the emptying of the niche leads to functional defects in the remaining cells.

Irf4 acts upstream of CD97

The transcription factor IRF4 has a well-studied but poorly understood role in promoting the normal accumulation and function of cDC2s (2, 7, 35, 36). Splenic cDC2s in mice lacking

IRF4 in CD11c^{+} cells (referred to as *Irf4*^{cKO}) shared many phenotypes with CD97 pathway-deficient cDC2s, including reduced frequency (Fig. 7A), reduced labeling by circulating antibody (Fig. 7B), increased cDC2s in blood (Fig. 7C), increased F-actin (Fig. 7D), and reduced F4/80 expression (fig. S9A). Mice deficient in lymphotoxin β receptor or EBI2 had reduced cDC2 frequencies (6, 9, 37) but exhibited normal F-actin content, F4/80 expression, and CD97 levels (fig. S9, B to E), which suggests that cDC2 deficiency itself does not cause the changes in these parameters. The abundance of CD97 on the splenic cDC2s remaining in IRF4-deficient mice was ~60% less than on WT cDC2s (Fig. 7E). Analysis of CD97 heterozygous mice showed that they had almost 50% reduced CD97 levels compared with WT cells (fig. S9F), and the cDC2s were slightly reduced in frequency (fig. S9G) and had detectably increased F-actin (fig. S9, H and I), indicating that splenic cDC2s have a dose-sensitive dependence on CD97. Thus, even a partial reduction in CD97 expression in the absence of IRF4 may contribute to the cDC2 deficiency in *Irf4*^{cKO} mice.

IRF4 binds the *Adgre5* promoter, as shown in chromatin immunoprecipitation sequencing analysis (38). RNA-sequencing (RNAseq) analysis confirmed that IRF4-deficient cDC2s had reduced expression of *Adgre5* (fig. S9J). GSEA showed that up-regulated and down-regulated genes in CD97-deficient cells were strongly enriched in IRF4-regulated genes (fig. S9K). These data are in accord with CD97 acting within the IRF4 gene-expression network. To further test the contribution of reduced CD97 expression to the *Irf4*^{cKO} phenotype, we sectively restored CD97 expression in IRF4-deficient BM chimeric mice. This led to a partial rescue in splenic cDC2s (Fig. 7, F and G). A difference between IRF4 deficiency and CD97 deficiency was the IRF4 requirement for normal accumulation of LN migratory cDC2s (fig. S9L) (39-42) that was not seen for the CD97 pathway (figs. S2G and S4F). IRF4 was not required for CD97 expression by LN migratory cDC2s, although it was needed for normal CD97 expression by LN-resident cDC2s (fig. S9, M and N). Thus, IRF4 is needed for the expression and function of the CD97 pathway in lymphoid tissue cDC2s, and this component of the IRF4 gene expression program accounts for essential features of the IRF4 requirement of splenic cDC2s.

Discussion

Our findings establish a role for an adhesion GPCR in promoting cell retention and function within the spleen. The adhesion GPCR family has 33 members, and the functions of only a small number of them are well understood. In most of these cases, activation occurs in a mechanosensitive manner–for example, through shear force-mediated removal of the NTF (16, 17, 43). The binding of CD97 to CD55 was first shown in vitro in the context of CD97-transfected cells binding RBCs, but the physiological relevance of this binding has been unclear (20). Our finding that CD97 is needed in splenic cDC2s for engagement by CD55^{+} RBCs, cells that cDC2s encounter in regions of blood flow, leads us to propose that the receptor acts in a mechanosensitive manner in cDC2s. We suggest that when cDC2s extend membrane processes into regions of blood flow, they sense their location through the exertion of pulling forces by RBC CD55 on cDC2 CD97. This leads to extraction of the NTF, exposure of the Stachel sequence, and activation of the GPCR domain, triggering a $G\alpha_{13}$-dependent membrane retraction pathway. These signals may also promote integrin-mediated adhesion (44, 45). Over time, when this pathway is lacking, not only

are cDC2s lost from the spleen, but the remaining cells upregulate their F-actin, and Mrtf transcription factors become active and drive expression of many cytoskeleton-associated genes. Although our study explains a requirement for splenic cDC2 retention in regions of blood flow, the mechanism used by some cDC1s to position in a similar location remains to be defined. We propose that the CD55–CD97–$G\alpha_{13}$–ArhGEF1 signaling pathway augments the ability of $IRF4^+$ cDC2s to present blood-borne particulate antigens by promoting cell positioning and cytoskeletal behaviors that facilite antigen capture and presentation. A number of mechanosensitive pathways have been identified that allow cells to sense exposure to blood flow (43). Our studies add an adhesion GPCR to the mechanosensitive molecular systems used by cells to sense their exposure to blood cells in regions of flow.

Materials and Methods

Mice

B6 (NCI 556) and B6-Ly5.2 (CD45.1) (NCI 564) mice were purchased from National Cancer Institute at Charles River at age 6-8 weeks. *Cd11c*-cre (MGI: 3763248) mice were provided by C. A. Lowell, University of California, San Francisco (UCSF). *Rag1*$^{-/-}$ (97848) mice were provided by A. Ma, UCSF. *Mpl*$^{-/-}$ mice were provided by M. R. Looney, UCSF. *Irf4*$^{f/f}$ mice (MGI: 3664434), *Tcrb*$^{-/-}$ mice (MGI:1857256) and CRISPR/Cas9 knock-in mice (026179) were purchased from The Jackson Laboratory. Ovalbumin (OVA)-specific TCR transgenic OT-II mice (MGI: 3046083), hen egg lysozyme (HEL)-specific immunoglobulin heavy chain knockin and light chain transgenic Hy10 mice, *Ebi2*$^{-/-}$ mice, and *Ltbr*$^{-/-}$ mice were from an internal colony. *Arhgef1*$^{-/-}$ mice (46) and *Gna13*$^{f/f}$ mice(47) were backcrossed to B6/J for 10 generations. *Adgre5*$^{-/-}$ mice and *Cd55*$^{-/-}$ mice were generated with CRISPR/Cas9 in C57BL/6J background, and the sequences of the guides were 5′-GTAAAATGCACACCACTGCA-3′ and 5′-GAGAGTGAGAATACATGTCA-3′ for *Adgre5* and 5′-CTGGCATTAGGAATGTCTGG-3′ and 5′-TCTGTCTTGAAAATGGCCAA-3′ for *CD55*. The CRISPR-EZ protocol (48) was followed with the main exception that the electroporation was performed twice. F0 founder mice were bred to C57BL/6J mice for two generations to avoid mosaicism and off-target effects. All mice were maintained under specific-pathogen-free conditions in the Laboratory of Animal Research Center at UCSF, and all animal procedures were approved by the UCSF Institutional Animal Use and Care Committee. For BM chimeras, mice were lethally irradiated by 550 rad γ-irradiation in two doses 3 hours apart and transferred intravenously with BM cells from donors of indicated genotypes. Chimeras were analyzed 5-10 weeks after reconstitution. In vivo labeling of blood-exposed cells was with 1 μg of PE-conjugated anti-CD45.2 (104, Biolegend) or anti-CD11c (N418, Biolegend) injected intravenously. Mice were then analyzed after 3 min. For CD97 or CD55 blockade, mice were treated with 40 μg of purified anti-CD97 (MAB33734, R&D) or 33 μg of purified anti-CD55 (RIKO-3, Biolegend) injected intravenously. Mice were then analyzed 2 days post treatment.

Retroviral constructs and transductions.

Gna13 and Arhgef1 retroviral constructs were made by inserting the murine open reading frame into the MSCV2.2 retroviral vector followed by an IRES and Thy1.1 as an expression marker. Adgre5 (1,2,X,3,4), Adgre5 (1,2,4) and its mutants, joined to Thy1.1 by a 2A

self-cleaving peptide sequence, were inserted into the pQEF MoMLV retroviral vector that incorporates an EF1 promoter for improved expression (49). Adgre5 (1,2,4) with a C-termial GFP fusion, was inserted into the pQEF MoMLV retroviral vector. For the G protein-coupled-receptor screen, single-guide RNA (sgRNA) sequences were cloned into the pTR-MSCV-IRES-Thy1.1 vector. sgRNA sequences were selected using Benchling's CRISPR Guide tool. For BM transduction, donor mice were injected intravenously with 3 mg of 5-fluorouracil (Sigma). BM was collected after 4 to 5 days and cultured with complete DMEM, supplemented with 20 ng/ml of interleukin-3 (IL-3), 50 ng/ml of IL-6, and 100 ng/ml of stem cell factor. BM cells were spin-infected (1000*g*, 2 hours, 32°C) at day 1 and day 2 and injected into irradiated recipients after the second infection.

Adoptive transfer and immunizations.

For analysis of OVA-specific OTII T cell response, 2×10^5 naïve CellTrace violet (CTV)-labeled OTII T cells were intravenously injected into mice and immunized with OVA-conjugated sheep blood cells (SRBCs). For OVA-SRBC conjugation (6), 1 ml of SRBCs was pelleted by centrifugation at 1000*g* for 5 min. One mililiter of PBS containing 30 mg/ml OVA with 25 mg EDC (1-ethyl-3-(3-dimethylaminopropyl)carbodiimide hydrochloride, ThermoFisher) was added to resuspend the pellet, and incubated for 1 hour on ice. For analysis of GC response, 1×10^5 naïe HEL-specific Hy10 B cells were adoptively transferred into recipients and immunized with SRBCs conjugated with low affinity HEL^{2x}. For conjugation of SRBC-HEL^{2x}, 1 ml of washed SRBCs was resuspended in 0.8 ml of PBS buffer, mixed with 0.1 ml of 0.2 mg/ml HEL^{2x} solution and 0.1 ml of 100 mg/ml EDC and incubated for 1 hour on ice. Conjugated SRBCs were washed three times to remove the free HEL^{2x}. For the SRBC uptake assay, 1 ml of SRBCs was resuspended with 1 ml of conjugation buffer with 4 μl of PKH26 dye for 20 min following the manual instruction. They were then washed three times with PBS. Eighty microliters of PKH26-labeled SRBCs was intravenously injected into each mouse 3 hours prior to analysis. Mice were immunized intravenously with 5×10^8 heat-inactivated *Listeria monocytogenes* (HKLM, InvivoGen) and analyzed for splenic GC reaction 8 days post immunization.

Dendritic cell ablation.

For DC ablation in *Zbtb46*$^{DTR/+}$: Adgre5 mixed BM chimeras, mice were injected intravenously with 25 ng of diphtheria toxin (DT, Sigma) per gram of body weight 2 days before transfer of OTII T cells or PKH26 labeled SRBCs. The mice were further treated intraperitoneally with 2.5 ng per gram of body weight DT on the day of cell transfer and 2 days after cell transfer to maintain ablation.

RBC alloimmunization model.

RBCs were collected from C57/B6 mice in Alsever's solution at 4°C. The cells were stored for 12 days before use as human RBC storage for this period has been shown to increase their allogenicity (34). Before transfusion, 1 ml of washed RBCs was added to 0.8 ml of PBS buffer, mixed with 0.1 ml of 0.5 mg/ml HEL-OVA solution and 0.1 ml of 100 mg/ml EDC and incubated for 1 hour on ice. Conjugated RBCs were washed three times to remove free HEL-OVA. Eighty microliters of HEL-OVA conjugated RBCs were intravenously transferred for alloantibody induction. Twenty-one days later, serum was

collected. To identify the presence of alloantibodies, sera were diluted 1:5 with PBS and incubated with 5 μl of HEL-OVA conjugated RBCs or unconjugated RBCs for 30 min on ice. After washing, the RBCs were stained with anti-mouse IgG conjugated with APC for 30 min on ice. The stained samples were washed and the total IgGs were detected by flow cytometry.

Immunofluorescent staining.

Ten-micron cryosections of spleen were fixed by acetone for 10 min, dried for 1 hour, and stained as described before. For DCIR2 staining, the tyramide amplification kit was used (TSA Biotin System, Perkin Elmer; Waltham, MA) according to the manual. Images were captured using a Zeiss AxioOberver Z1 inverted microscope with Zeiss AxioCam 506 mono and Zeiss Plan-Apochromat 10X/0.45 objective len. Images were processed and stitched by Zeiss ZEN 2 (blue edition) software.

Flow cytometry.

Single-cell splenocyte suspensions were washed, blocked with 2.4G2 antibody (Bio X cell), and stained with antibodies of indicated specificities in MACS buffer (PBS+1% FBS). Staining reagents include: BV786-conjugated anti-B220 (RA3-6B2), eFluor450-conjugated anti-CD8a (53-6.7), PerCP/Cy5.5-conjugated anti-MHCII (M5/114.15.2), APC-conjugated anti-DCIR2 (33D1), PE/Cy7-conjugated anti-CD279 (RMP1-30), PE-conjugated anti-CD45.2 (104), biotinylated-conjugated anti-DCIR2 (33D1), biotinylated-conjugated anti-CCR7 (4B12), BV711-conjugated anti-CD4 (GK1.5), PE-conjugated anti-CD278 (15F9), PE/Cy7-conjugated anti-CD95 (SA367H8), Pacific Blue-conjugated anti-GL7 (GL7), PE-conjugated anti-CD135 (A2F10), APC-conjugated anti-CD172a (P84) and BV605-conjugated anti-CD86 (GL-1) from Biolegend; FITC-conjugated anti-Vα2 TCR (B20.1), streptavidin-BV711 and streptavidin-BV605 from BD Biosciences; PE/Cy7-conjugated anti-CD11c (N418) from Tonbo Bio; PE-conjugated anti-CD55 (REA300) and APC-conjugated anti-CD97 (REA678) from Miltenyibiotec. HEL was conjugated with Alexa Fluor 647 by Alexa Fluor 647 Antibody Labeling Kit (A20186) from Thermo Fisher. All antibodies were used at a 1:200 dilution except for those against CCR7, CD97, and CD55, which were used at a 1:100 dilution. Dead-cell exclusion was based on Fixable Viability Dye eFluor 780 staining (eBioscience) and non-singlet events were excluded with FSC-W/FSC-H characteristics. All data were collected on an LSR II cytometer (BD Biosciences) and analyzed with FlowJo software (TreeStar).

EdU labeling and analysis.

For short-term EdU labeling, mice were treated intravenously with 1 mg of 5-ethynyl-2′-deoxyuridine (EdU) 45 min before being sacrificed. Cells were stained for incorporated EdU with the Click-iT EdU Alexa Fluor 647 Flow Cytometry Assay Kit (Invitrogen) according to the manufacturer's instructions.

Red blood cell enrichment and transfusion.

Five hundred microliters of blood was collected retro-orbitally from *CD55*$^{-/-}$ or *CD55*$^{+/+}$ mice into Alsever's solution. The blood was mixed followed by 100*g* centrifugation for

15 min at room temperature. The platelet-rich plasma and leukocyte-rich buffy coat were removed. Then *Cd55*$^{-/-}$ or *Cd55*$^{+/+}$ RBCs were intravenously transferred into appropriate mice from which 500 μl of blood had previously been removed. For WBC transfer, 500 μl of blood from *Cd55*$^{-/-}$ or *Cd55*$^{+/+}$ mice was lysed by ACK buffer. WBCs were then transferred into recipients with indicated genotypes. Mice were analyzed 6-8 days post blood transfusion.

CD97 isoforms detection.

cDC2s and cDC1s were enriched by CD11c MicroBeads from Miltenyi Biotec, and then sorted with an Aria III (BD Biosciences). CD97 isoforms were detected by polymerase chain reaction. The following primers were used: P1, 5′-CAGGAGCTGGAACCCAGAAG-3’; P2, 5′-GGTGGCTCTTGGCATATGGT-3′.

Shear flow model in vitro.

To mimic shear flow in vitro, 900 μl of blood were collected from *Cd55*$^{+/+}$ or *Cd55*$^{-/-}$ mice in 100 μl of Alsever's solution, and the blood was mixed followed by 100*g*-centrifugation for 15 min at room temperature to separate RBCs from the white blood cells. 100 μl of the lower RBC fraction was added to 2×10^6 splenocytes from *Cd55*$^{-/-}$, *Cd55*$^{+/+}$, or CD97-mutant mice in 1.5-ml tubes and shaken (Eppendorf-ThermoMixer F1.5) at RT at 900 rpm (shear ~12.5 dyne/cm^2 (50)) or not agitated. After 1 hour, cells were harvested, lysed, and analyzed by flow cytometry for CD97 expression.

IVC surgery.

Cd55$^{+/+}$ or *Cd55*$^{-/-}$ mice were anesthetized with isoflurane. A midline abdominal incision was made to expose the portal vein, the IVC and the aorta. Three 7-0 silk sutures were placed under the three vessels prepared for ligation. Donor *Cd55*$^{-/-}$ splenocytes were harvested and stained with CellTrace Violet. Twenty units of heparin was injected retroorbitally. Five minutes later, labeled *Cd55*$^{-/-}$ splenocytes were intravenously transferred into recipients. Fifteen seconds later, the portal vein, the IVC and the aorta were ligated. Blood from the distal IVC and heart was collected 30 min after vessel ligation.

Mouse spleen transplantation.

Mouse spleen transplantation was performed as previously described (51). Donor chimeras CD45.1 WT: CD45.2 *Gna13*^{WT} or CD45.1 WT: CD45.2 *Gna13*^{cKO} were anesthetized with isoflurane. A midline abdominal incision was made to expose the spleen. The short gastric vein, superior pancreaticoduodenal vein, and left gastric vessels were ligated with 7-0 silk suture. Part of the portal vein connecting with the splenic vein and the abdominal aorta near the celiac truck were dissected and mobilized. Then 50 units of heparin was injected into the IVC. The portal vein distal to the splenic vein and the aorta above celiac trunk were ligated with a 7-0 suture, respectively. The spleen was perfused with 3 to 4 ml of cold heparinized saline (4°C, 100 U/ml) through the abdominal aorta. The splenic artery–celiac trunk–abdominal aorta patch was prepared by transecting the aorta below the celiac trunk. The splenic vein–portal vein patch was prepared by transecting the portal vein proximal to the liver. The spleen graft was then removed and preserved in cold

saline (4°C). For the CD45.1/CD45.2 recipients, the aorta, and the IVC were crossclamped using two microvascular clips. The splenic artery–celiac trunk–abdominal aorta patch was anastomosed to the recipient aorta and the splenic vein-portal vein patch was anastomosed to the recipient IVC using 11-0 sutures. The microvascular clips were removed to perfuse the donor spleen. The native splenic artery and vein were occluded by 7-0 suture and the recipient native spleen was removed. Finally the abdomen was closed with 6-0 suture. Eight to nine hours later, blood and spleens were collected to analyze the B cell and cDC2 compartments.

RNA-seq and GSEA.

Spleens were digested with type IV collagenase and deoxyribonuclease I for 10 min and mashed into single cell suspension. DCs were enriched with anti-CD11c microbeads (Miltenyi Biotec) and sorted on an AriaIII from BD Biosciences. Total RNA was purified from sorted cells using the RNeasy Micro kit (Qiagen). RNA quality was assessed with an Agilent 2100 Bioanalyzer. Barcoded sequencing libraries were generated with the Ovation RNA-Seq System V2 (Nugen), a KAPA HyperPrep Kit for Illumina (KAPA Biosystems) and NEXTflex DNA barcodes. Single-end sequencing was performed on an Illumina HiSeq 4000 in the UCSF Center for Advanced Technology. Sequences were aligned to the mm10 genome with STAR. HTseq was used to count the mapped reads of each gene and DESeq2 was used for the gene differential expression analysis. lfcShrink function of DESeq2 is used to calculate the shrunken log2-fold changes. plotMA function of DESeq2 is used to generate the MA plot. Points are colored blue if the adjusted *P* value of shrunken log2-fold change is less than 0.1. Points which fall out of the window are plotted as open triangles pointing either up or down. GSEA analysis was carried out using the GSEA software. *P*adj<0.001 was used as the threshold to define the significantly differentially expressed genes. For each comparison, the rank file was generated with the fcros-package for subsequent pre-ranked GSEA analysis. The significantly up- or downregulated genes were compared to the pre-ranked files. GSE77671 was used to compare CD97 regulated genes in mice with splenic human dendritic cells (24). Genes that were downregulated by *Mrtfa*$^{-/-}$ BMDCs cells (29) were used as the test gene sets for enrichment analysis. Raw RNA-seq data are available from the GEO under the accession number GSE188835.

Intravital imaging of DCs in spleen.

Splenic DCs were imaged with *Arhgef1*$^{+/-}$ *Batf3*$^{-/-}$ *Cd11c*-YFP and *Arhgef1*$^{-/-}$ *Batf3*$^{-/-}$ *Cd11c*-YFP chimeras. In some cases, 0.5 mg of 155-kDa dextran-TRITC in 200 μl of PBS was intravenously injected 30 min prior to imaging. The basic setup and procedure for intravital two-photon imaging of mouse spleens were essentially the same as previously described (10). Images were conducted with ZEN2012 (Carl Zeiss) using a 7MP two-photon microscope equipped with a Chameleon laser, Zeiss INDIMO 4 channel GaAsP detector system and W Plan-Apochromat 20X/1.0 objective len at a *z*-step of 3 μm. The imaging depth under the capsule of the spleen was between ~50 μm and ~150 μm. For video acquisition, a series of images were collected every 20 s. Excitation wavelengths were 830-860 nm. Emission filters were 500-550 nm for YFP, and 570-640 nm for TRITC. Off-line analyses were conducted with Imaris software (Bitplane). Cell count was analyzed with Imaris automatic spot tracking aided by manual verification, and cell migration was

analyzed and verified with manual tracking in 3D views. The surface of large blood vessels was created according to dextran-Tritic signaling. Spots and tracks that lasted less than 1 min were excluded from analysis. Migratory cDC2s were defined as cells with at least a 30-μm track length across the imaging period. The mean imaging period for both types of chimeras was 45 min (number of movies analyzed: 25 *Arhgef1*$^{+/-}$ *Batf3*$^{-/-}$ *Cd11c*-YFP and 29 *Arhgef1*$^{-/-}$ *Batf3*$^{-/-}$ *Cd11c*-YFP). Image sequences were annotated in Adobe PhotoShop when necessary and rendered as movies with Adobe AfterEffect. All movies are played back at 20 frames per second (fps) unless indicated otherwise, and time stamps are minutes:seconds.

Statistical analysis.

Statistical analysis and graphing were performed using Prism 9.0 (GraphPad). Two-tailed Student's *t* tests were used to compare endpoint means of different groups. In grouped analysis, ordinary two-way analysis of variance (ANOVA) was performed and the *P* values indicated are from individual *t* tests with Sidak's multiple test correction. When multiple comparisons were being performed, ordinary one-way ANOVA with Dunnett's multiple comparisons was used.

Supplementary Material

Refer to Web version on PubMed Central for supplementary material.

Acknowledgements:

We thank S. Coughlin for *ArhGEF1*- and *Gna13*-deficient mice and R. Brink for HEL^{2x}. We thank M. De Giovanni for advice regarding imaging analysis, J. Muppidi and X. Piao for helpful discussions, and N. Carey for advice on statistical analysis.

Funding:

D.L. was supported by an Cancer Research Institute Irvington Fellowship and by funds from the UCSF Helen Diller Family Comprehensive Cancer Center. E.L. was supported by NSF grant 1144247. A.M. holds a Career Award for Medical Scientists from the Burroughs Wellcome Fund and a Lloyd J. Old STAR award from the Cancer Research Institute, is an investigator at the Chan Zuckerberg Biohub, and received funds from Parker Institute for Cancer Immunotherapy and the Innovative Genomics Institute. Z.Y and C.A. were supported by funds from The Sandler Asthma Basic Research Center. J.G.C. is an investigator of the Howard Hughes Medical Institute. This work was supported in part by NIH grant AI040098 to JGC.

References and Notes:

1. Eisenbarth SC, Dendritic cell subsets in T cell programming: location dictates function. Nat. Rev. Immunol 19, 89–103 (2019). [PubMed: 30464294]
2. Anderson DA 3rd, Dutertre CA, Ginhoux F, Murphy KM, Genetic models of human and mouse dendritic cell development and function. Nat. Rev. Immunol, (2020).
3. Mebius RE, Kraal G, Structure and function of the spleen. Nat. Rev. Immunol 5, 606–616 (2005). [PubMed: 16056254]
4. Yamamoto K, Kobayashi T, Murakami T, Arterial terminals in the rat spleen as demonstrated by scanning electron microscopy of vascular casts. Scan. Electron Microsc. Pt 1, 455–458. (1982). [PubMed: 7167761]
5. Schmidt EE, MacDonald IC, Groom AC, Comparative aspects of splenic microcirculatory pathways in mammals: the region bordering the white pulp. Scanning Microsc. 7, 613–628. (1993). [PubMed: 8108677]

6. Yi T, Cyster JG, EBI2-mediated bridging channel positioning supports splenic dendritic cell homeostasis and particulate antigen capture. Elife 2, e00757 (2013). [PubMed: 23682316]
7. Calabro S et al. , Differential Intrasplenic Migration of Dendritic Cell Subsets Tailors Adaptive Immunity. Cell Rep 16, 2472–2485 (2016). [PubMed: 27545885]
8. Lu E, Dang EV, Cyster JG, Distinct oxysterol requirements for positioning naive and activated dendritic cells in the spleen. Science Immunology 2, eaal5237 (2017). [PubMed: 28738017]
9. Liu D, Wu J, An J, Cyster JG, Requirements for cDC2 positioning in blood-exposed regions of the neonatal and adult spleen. J. Exp. Med 217, e20192300 (2020). [PubMed: 32808016]
10. Arnon TI, Horton RM, Grigorova IL, Cyster JG, Visualization of splenic marginal zone B-cell shuttling and follicular B-cell egress. Nature 493, 684–688 (2013). [PubMed: 23263181]
11. Gatto D et al. , The chemotactic receptor EBI2 regulates the homeostasis, localization and immunological function of splenic dendritic cells. Nat. Immunol 14, 446–453 (2013). [PubMed: 23502855]
12. Worzfeld T, Wettschureck N, Offermanns S, G(12)/G(13)-mediated signalling in mammalian physiology and disease. Trends Pharmacol. Sci. 29, 582–589 (2008). [PubMed: 18814923]
13. Lu E, Cyster JG, G-protein coupled receptors and ligands that organize humoral immune responses. Immunol. Rev. 289, 158–172 (2019). [PubMed: 30977196]
14. Lewis KL et al. , Notch2 receptor signaling controls functional differentiation of dendritic cells in the spleen and intestine. Immunity 35, 780–791 (2011). [PubMed: 22018469]
15. Langenhan T, Aust G, Hamann J, Sticky signaling--adhesion class G protein-coupled receptors take the stage. Sci Signal 6, re3 (2013). [PubMed: 23695165]
16. Purcell RH, Hall RA, Adhesion G Protein-Coupled Receptors as Drug Targets. Annu. Rev. Pharmacol. Toxicol. 58, 429–449 (2018). [PubMed: 28968187]
17. Vizurraga A, Adhikari R, Yeung J, Yu M, Tall GG, Mechanisms of adhesion G protein-coupled receptor activation. J. Biol. Chem. 295, 14065–14083 (2020). [PubMed: 32763969]
18. Leemans JC et al. , The epidermal growth factor-seven transmembrane (EGF-TM7) receptor CD97 is required for neutrophil migration and host defense. J. Immunol 172, 1125–1131 (2004). [PubMed: 14707087]
19. Dho SH, Lim JC, Kim LK, Beyond the Role of CD55 as a Complement Component. Immune Netw 18, e11 (2018). [PubMed: 29503741]
20. Hamann J, Vogel B, van Schijndel GM, van Lier RA, The seven-span transmembrane receptor CD97 has a cellular ligand (CD55, DAF). J. Exp. Med 184, 1185–1189 (1996). [PubMed: 9064337]
21. Hilbig D et al. , Mechano-Dependent Phosphorylation of the PDZ-Binding Motif of CD97/ADGRE5 Modulates Cellular Detachment. Cell Rep 24, 1986–1995 (2018). [PubMed: 30134161]
22. Hsiao CC et al. , CD97 inhibits cell migration in human fibrosarcoma cells by modulating TIMP-2/MT1- MMP/MMP-2 activity--role of GPS autoproteolysis and functional cooperation between the N- and C-terminal fragments. FEBS J. 281, 4878–4891 (2014). [PubMed: 25174588]
23. Liebscher I et al. , A tethered agonist within the ectodomain activates the adhesion G protein-coupled receptors GPR126 and GPR133. Cell Rep 9, 2018–2026 (2014). [PubMed: 25533341]
24. Heidkamp GF et al. , Human lymphoid organ dendritic cell identity is predominantly dictated by ontogeny, not tissue microenvironment. Sci Immunol 1, (2016).
25. Russell ES, Bernstein SE, in Biology of the Laboratory Mouse, Green EL, Ed. (DOVER PUBLICATIONS, INC., NEW YORK, 1966), vol. 2, chap. 17.
26. Karpus ON et al. , Shear stress-dependent downregulation of the adhesion-G protein-coupled receptor CD97 on circulating leukocytes upon contact with its ligand CD55. J. Immunol 190, 3740–3748 (2013). [PubMed: 23447688]
27. Posern G, Treisman R, Actin' together: serum response factor, its cofactors and the link to signal transduction. Trends Cell Biol. 16, 588–596 (2006). [PubMed: 17035020]
28. Gau D, Roy P, SRF'ing and SAP'ing - the role of MRTF proteins in cell migration. J. Cell Sci 131, (2018).

29. Guenther C et al. , A beta2-Integrin/MRTF-A/SRF Pathway Regulates Dendritic Cell Gene Expression, Adhesion, and Traction Force Generation. Front Immunol 10, 1138 (2019). [PubMed: 31191527]
30. Costello P et al. , MRTF-SRF signaling is required for seeding of HSC/Ps in bone marrow during development. Blood 125, 1244–1255 (2015). [PubMed: 25573994]
31. Hildner K et al. , Batf3 deficiency reveals a critical role for CD8alpha+ dendritic cells in cytotoxic T cell immunity. Science 322, 1097–1100 (2008). [PubMed: 19008445]
32. Arasa J, Collado-Diaz V, Halin C, Structure and Immune Function of Afferent Lymphatics and Their Mechanistic Contribution to Dendritic Cell and T Cell Trafficking. Cells 10, (2021).
33. Briseno CG et al. , Notch2-dependent DC2s mediate splenic germinal center responses. Proc. Natl. Acad. Sci. U. S. A 115, 10726–10731 (2018). [PubMed: 30279176]
34. Hendrickson JE, Hod EA, Spitalnik SL, Hillyer CD, Zimring JC, Storage of murine red blood cells enhances alloantibody responses to an erythroid-specific model antigen. Transfusion (Paris) 50, 642–648 (2010).
35. Persson EK et al. , IRF4 transcription-factor-dependent CD103(+)CD11b(+) dendritic cells drive mucosal T helper 17 cell differentiation. Immunity 38, 958–969 (2013). [PubMed: 23664832]
36. Li J, Lu E, Yi T, Cyster JG, EBI2 augments Tfh cell fate by promoting interaction with IL-2-quenching dendritic cells. Nature 533, 110–114 (2016). [PubMed: 27147029]
37. Kabashima K et al. , Intrinsic Lymphotoxin-beta Receptor Requirement for Homeostasis of Lymphoid Tissue Dendritic Cells. Immunity 22, 439–450 (2005). [PubMed: 15845449]
38. ENCODE Project Consortium, An integrated encyclopedia of DNA elements in the human genome. Nature 489, 57–74 (2012). [PubMed: 22955616]
39. Bajana S, Roach K, Turner S, Paul J, Kovats S, IRF4 promotes cutaneous dendritic cell migration to lymph nodes during homeostasis and inflammation. J. Immunol 189, 3368–3377 (2012). [PubMed: 22933627]
40. Gao Y et al. , Control of T helper 2 responses by transcription factor IRF4-dependent dendritic cells. Immunity 39, 722–732 (2013). [PubMed: 24076050]
41. Tussiwand R et al. , Klf4 expression in conventional dendritic cells is required for T helper 2 cell responses. Immunity 42, 916–928 (2015). [PubMed: 25992862]
42. Krishnaswamy JK et al. , Migratory CD11b(+) conventional dendritic cells induce T follicular helper cell-dependent antibody responses. Sci Immunol 2, eaam9169 (2017). [PubMed: 29196450]
43. Scholz N, Monk KR, Kittel RJ, Langenhan T, Adhesion GPCRs as a Putative Class of Metabotropic Mechanosensors. Handb Exp Pharmacol 234, 221–247 (2016). [PubMed: 27832490]
44. Laudanna C, Campbell JJ, Butcher EC, Role of Rho in chemoattractant-activated leukocyte adhesion through integrins. Science 271, 981–983. (1996). [PubMed: 8584934]
45. Yeung J et al. , GPR56/ADGRG1 is a platelet collagen-responsive GPCR and hemostatic sensor of shear force. Proc. Natl. Acad. Sci. U. S. A 117, 28275–28286 (2020). [PubMed: 33097663]
46. Francis SA, Shen X, Young JB, Kaul P, Lerner DJ, Rho GEF Lsc is required for normal polarization, migration, and adhesion of formyl-peptide-stimulated neutrophils. Blood 107, 1627–1635 (2006). [PubMed: 16263795]
47. Ruppel KM et al. , Essential role for Galpha13 in endothelial cells during embryonic development. Proc. Natl. Acad. Sci. U. S. A 102, 8281–8286 (2005). [PubMed: 15919816]
48. Chen S, Lee B, Lee AY, Modzelewski AJ, He L, Highly Efficient Mouse Genome Editing by CRISPR Ribonucleoprotein Electroporation of Zygotes. J. Biol. Chem 291, 14457–14467 (2016). [PubMed: 27151215]
49. Yang Z, Allen CDC, Expression of Exogenous Genes in Murine Primary B Cells and B Cell Lines Using Retroviral Vectors. Methods Mol. Biol 1707, 39–49 (2018). [PubMed: 29388098]
50. Ley K, Lundgren E, Berger E, Arfors KE, Shear-dependent inhibition of granulocyte adhesion to cultured endothelium by dextran sulfate. Blood 73, 1324–1330 (1989). [PubMed: 2467707]
51. Wang JJ et al. , A Mouse Model of Vascularized Heterotopic Spleen Transplantation for Studying Spleen Cell Biology and Transplant Immunity. J Vis Exp, (2019).

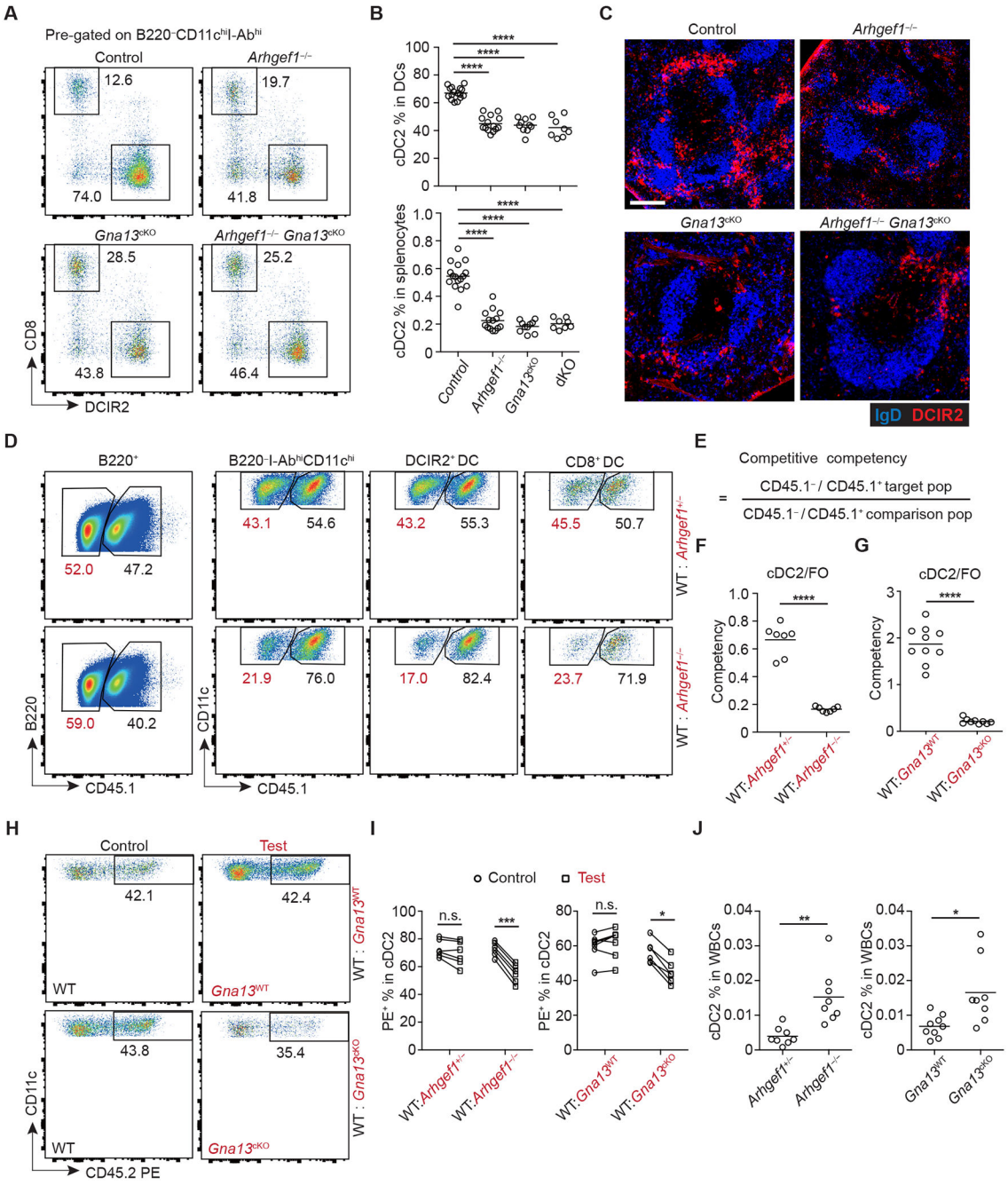

Fig. 1. Gα$_{13}$-ArhGEF1 signaling pathway is required in splenic cDC2s.

(**A** and **B**) Representative (A) flow cytometry profiles and (B) frequencies of DCIR2^{+}CD8^{-} cDC2s in total B220^{-}CD11c^{hi}I-Ab^{hi} DCs and (bottom) total splenocytes in *Arhgef1*$^{-/-}$, *Cd11c*-cre *Gna13*$^{fl/fl}$ (labeled as *Gna13*^{cKO}), *Arhgef1*$^{-/-}$ *Cd11c*-cre *Gna13*$^{fl/fl}$ (labeled as *Arhgef1*$^{-/-}$*Gna13*^{cKO} or dKO), and control mice. Data are pooled from three independent experiments. (**C**) Representative distribution patterns of DCIR2^{+} cDC2s (red) relative to B cells [immunoglobulin D (IgD), blue] in spleens of mice of the indicated genotypes. Scale bar, 200 μm. Sections are representative of multiple cross sections from at least three mice of each type. (**D** to **F**) Mixed (50:50) BM chimeras were made with CD45.1

WT (*Arhgef1*$^{+/+}$) and CD45.2 *Arhgef1*$^{+/-}$ or *Arhgef1*$^{-/-}$ BM cells. (D) Representative flow cytometry profiles show gating strategies. (E) Equation for calculating the competitive competencies of CD45.2^{+} (gated as CD45.1^{-}) population. (F) Plots showing CD45.2^{+} competency values in individual chimeras for the cDC2 compartment compared to B220^{+} follicular (FO) B cells. (**G**) Plots showing CD45.2^{+} competency values in WT:*Gna13*^{WT} and WT:*Gna13*^{cKO} chimeras for the cDC2 compartment compared to B220^{+} follicular (FO) B cells. (**H**) Flow cytometry profiles and (**I**) frequencies of in vivo anti-CD45-PE labeled cDC2s of indicated genotyped cells in (left) WT: *Arhgef1*$^{-/-}$ or WT: (right) *Gna13*^{cKO} and their control mixed BM chimeras. Lines connect data from same animals. (**J**) Frequencies of cDC2s in blood of (left) *Arhgef1*$^{-/-}$ or (right) *Gna13*^{cKO} and their control mice. In (D) to (J), data are pooled from two independent experiments. Each symbol represents one mouse and lines denote means. * $P<0.05$; ** $P<0.01$; *** $P<0.001$; **** $P<0.0001$.

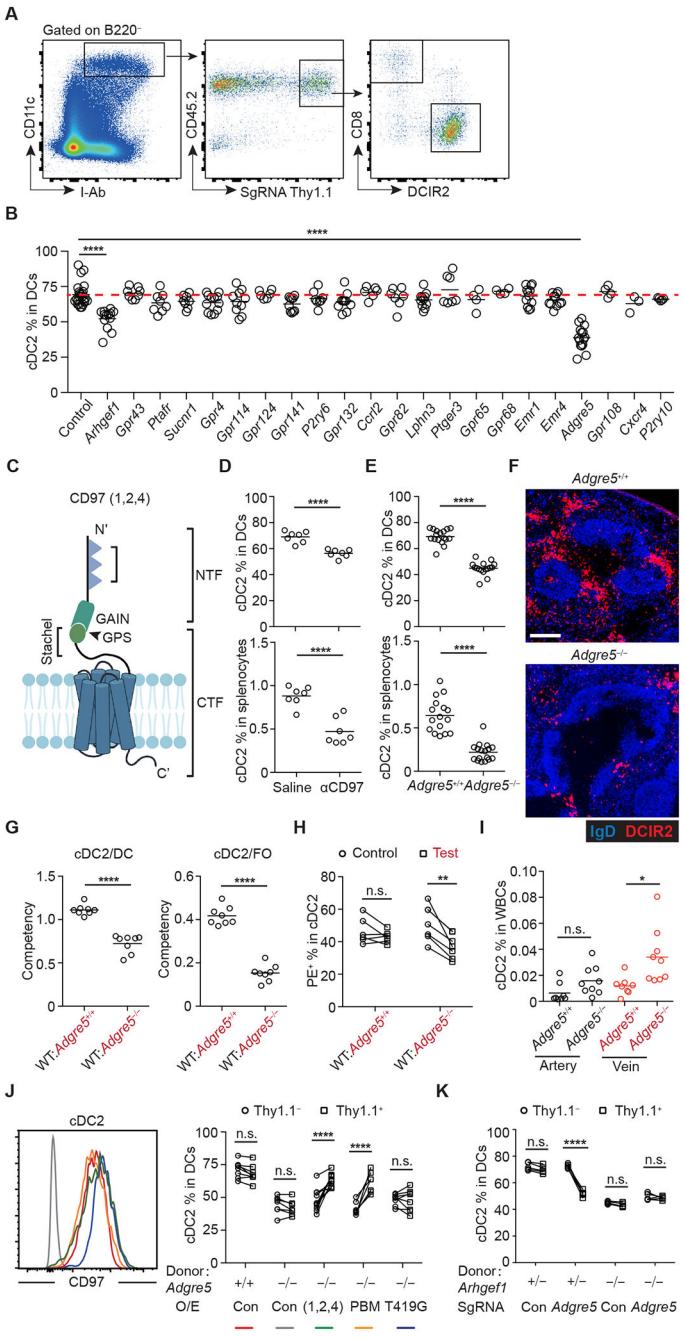

Fig. 2. CD97 functions upstream of $G\alpha_{13}$-ArhGEF1 in splenic cDC2s.

(**A** and **B**) Cas9-based mutagenesis screen was performed by making chimeras reconstituted with Cas9-expressing BM cells transduced with sgRNA targeting specific genes, with Thy1.1 as a reporter. (A) Gating strategy for the screen. (B) Frequencies of cDC2s in sgRNA-Thy1.1$^+$ DCs of chimeras with sgRNA targeting the indicated genes. Data are pooled from eight independent experiments. (**C**) Structural components of the CD97 short isoform. NTF, N-terminal fragment; CTF, C-terminal fragment; GAIN, GPCR autoproteolysis-inducing domain; GPS, GPCR proteolysis site; Stachel, putative tethered agonist peptide. Triangles indicate individual EGF domains. (**D**) Frequencies of cDC2s

in (top) total DCs and (bottom) total splenocytes in WT mice treated with antibody to CD97 antibody or saline. (**E**) Frequencies of cDC2s in (top) total DCs and (bottom) total splenocytes in *Adgre5*$^{+/+}$ or *Adgre5*$^{-/-}$ mice. Data are pooled from four independent experiments. (**F**) Representative distribution of DCIR2^{+} cDC2s (red) relative to B cells (IgD, blue) in spleens of *Adgre5*$^{+/+}$ or *Adgre5*$^{-/-}$ mice. Scale bar, 200 μm. Sections are representative of multiple cross-sections from at least three mice of each type. (**G** and **H**) Mixed (50:50) BM chimeras were made with CD45.1 WT and CD45.2 *Adgre5*$^{+/+}$ or *Adgre5*$^{-/-}$ BM cells. (G) The plots show CD45.2^{+} competency values in individual chimera for the cDC2 compartment compared with (left) total DCs or (right) B220^{+} follicular B (FO) cells. (H) Frequencies of in vivo anti-CD45-PE labeled cDC2s of indicated genotyped cells in mixed BM chimeras. (**I**) Frequencies of cDC2s in blood of *Adgre5*$^{-/-}$ and control mice. Artery means blood was collected from celiac artery near splenic artery. Vein means blood was collected from portal vein after ligation of superior mesenteric vein. (**J**) BM chimeras were reconstituted with *Adgre5*$^{+/+}$ or *Adgre5*$^{-/-}$ BM cells transduced with a retroviral construct encoding Adgre5 (1,2,4) or its mutants or empty vector, with Thy1.1 as a reporter. (Left) Representative histogram plots of surface CD97 on Thy1.1^{+} cDC2 cells in chimeras reconstituted as indicated. (Right) Color coding of histograms is as labeled in graph. Gray indicates isotype control. Frequencies of cDC2s in Thy1.1^{+} or Thy1.1^{-} DCs of chimeras reconstituted as indicated. In (G) to (J), data are pooled from two independent experiments. (**K**) Frequencies of cDC2s in sgRNA-Thy1.1^{+} or Thy1.1^{-} DCs of chimeras reconstituted with indicated genotyped BM cells transduced with sgRNA targeting *Adgre5* or control. One of two independent experiments with similar results is shown. In (B), (D), (E), (G), and (I), each symbol represents one mouse and lines denote means. In (H), (J), and (K), lines connect data from same animals. * P<0.05; ** P<0.01; **** P<0.0001.

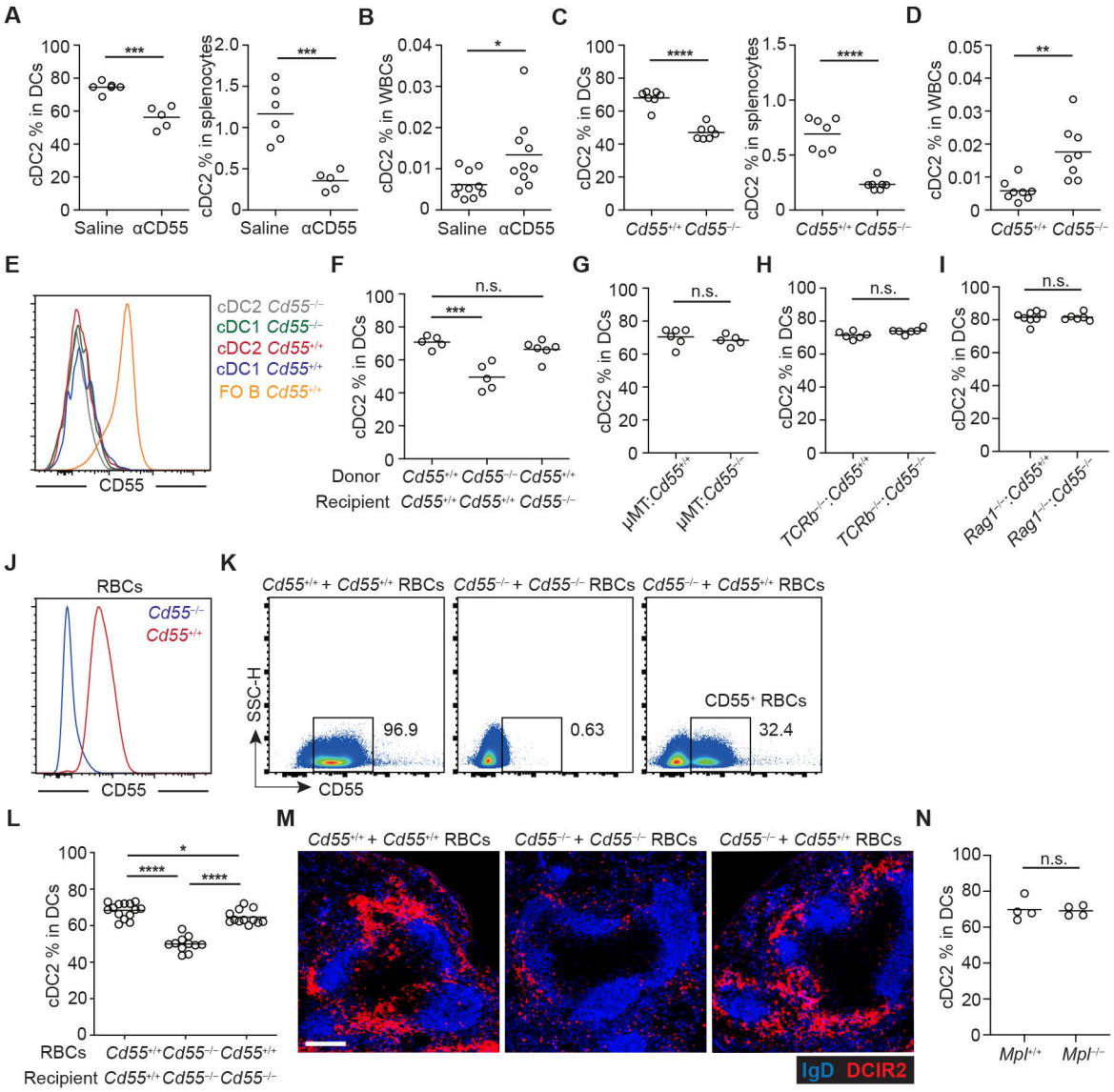

Fig. 3. CD55 on RBCs is required for splenic cDC2 homeostasis.

(**A**) Frequencies of cDC2s in (left) total DCs and (right) total splenocytes in WT mice treated with antibody to CD55 or saline. (**B**) Frequencies of cDC2s in blood of WT mice 8 hours after treatment with antibody to CD55 or saline. (**C**) Frequencies of cDC2s in (left) total DCs and (right) total splenocytes in *Cd55*$^{+/+}$ or *Cd55*$^{-/-}$ mice. (**D**) Frequencies of cDC2s in blood of *Cd55*$^{-/-}$ and control mice. (**E**) Representative histogram plots of surface CD55 on cDC2s, cDC1s, and B cells in mice with indicated genotype. (**F**) Frequencies of cDC2s in total DCs in chimeras as indicated. (**G**) Frequencies of cDC2s in total DCs in chimeras reconstituted with 90% μMT (IgM null) and 10% *Cd55*$^{+/+}$ or *Cd55*$^{-/-}$ BM cells. (**H**) Frequencies of cDC2s in total DCs in chimeras reconstituted with 90% *Tcrb*$^{-/-}$ and 10% *Cd55*$^{+/+}$ or *Cd55*$^{-/-}$ BM cells. (**I**) Frequencies of cDC2s in total DCs in chimeras reconstituted with 90% *Rag1*$^{-/-}$ and 10% *Cd55*$^{+/+}$ or *Cd55*$^{-/-}$ BM cells. In (A) to (I), data are pooled from two independent experiments. (**J**) Representative histogram plots of surface CD55 on RBCs in mice with indicated genotype. (**K** to **M**) RBC transfusions were

performed from *Cd55*$^{-/-}$ or *Cd55*$^{+/+}$ mice into the indicated recipient mice, and analysis was after 6 to 8 days. (K) Representative profile of purified *Cd55*$^{+/+}$ RBCs or *Cd55*$^{-/-}$ RBCs transfused into *Cd55*$^{-/-}$ or *Cd55*$^{+/+}$ recipients. (L) Frequencies of cDC2s in total DCs in mice with purified RBCs transfused as indicated. Data are pooled from three independent experiments. (M) Distribution of DCIR2^{+} cDC2s (red) and B cells (IgD, blue) in spleens as indicated. Scale bar, 200 μm. Representative of multiple cross sections from at least three mice of each type. (**N**) Frequencies of cDC2s in total DCs in *Mpl*$^{+/+}$ or *Mpl*$^{-/-}$ mice. Data are pooled from two independent experiments. Each symbol indicates one mouse, and lines denote means. * $P<0.05$; ** $P<0.01$; *** $P<0.001$; **** $P<0.0001$.

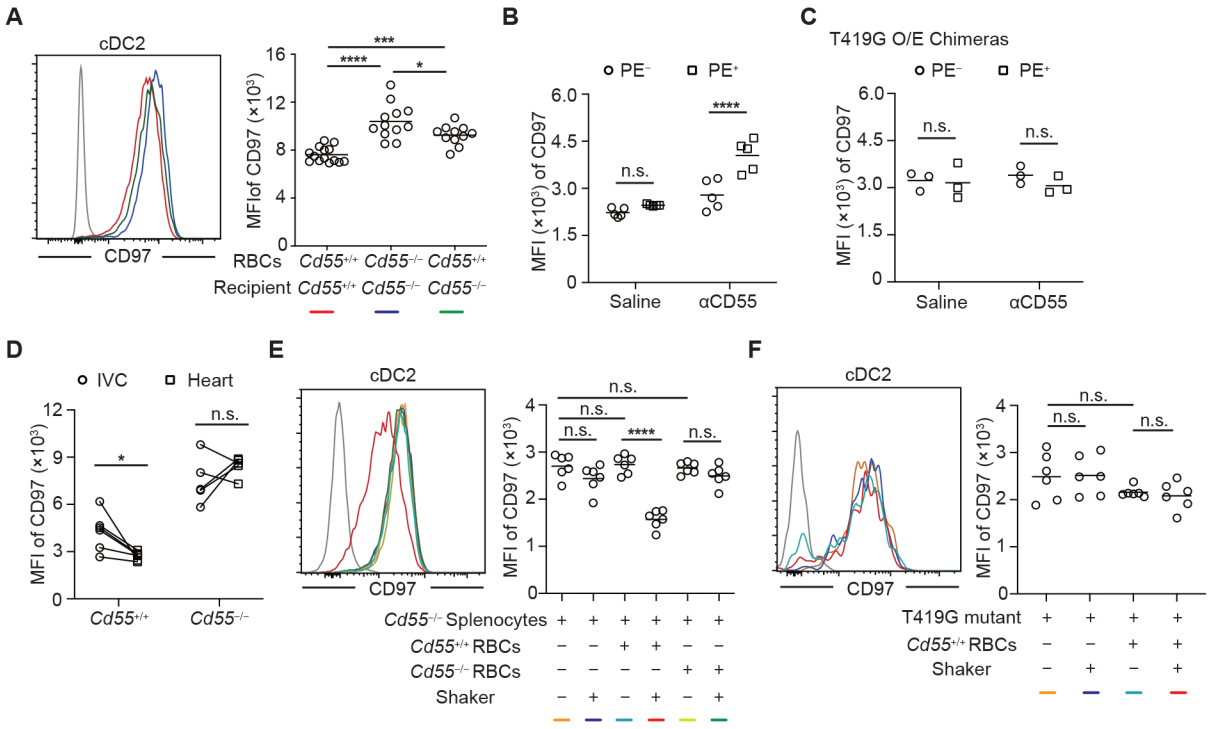

Fig. 4. CD55-mediated CD97 NTF extraction is dependent on shear stress.

(**A**) Representative (left) histogram and (right) geometric mean fluorescence intensity (MFI) of surface CD97 expression on cDC2s in mice with blood transfusion as indicated. Data are pooled from three independent experiments. (**B**) MFI of surface CD97 on in vivo PE labeled (PE^+) and PE non-labeled (PE^-) cDC2s in WT mice that had been treated 8 hours earlier with antibody to CD55 or saline. Data are pooled from two independent experiments. (**C**) Chimeras were reconstituted with *Adgre5*$^{-/-}$ BM transduced with Adgre5 (1,2,4)-T419G mutant, with Thy1.1 as a reporter. MFI of surface CD97 on in vivo PE labeled (PE^+) and PE non-labeled (PE^-) $Thy1.1^+$ cDC2s in chimeras that had been treated 8 hours earlier with antibody to CD55 or saline. One of two independent experiments with similar results is shown. (**D**) MFI of surface CD97 expression on transferred *Cd55*$^{-/-}$ cDC2s in blood collected from heart and distal ligated IVC of recipients as indicated (movie S1). Data are pooled from two independent experiments. (**E** and **F**) Splenocytes from (E) *Cd55*$^{-/-}$ mice or (F) CD97 T419G expressing BM chimeras were cocultured for 1 hour at RT with *Cd55*$^{-/-}$ or *Cd55*$^{+/+}$ RBCs, on a shaker or not. Representative (left) histogram and (right) MFI of surface CD97 expression on cDC2s are shown. Data are pooled from two independent experiments. In (A), (E), and (F), color coding of histograms is as for graphs, and gray lines indicate isotype control. In (A) to (C), (E), and (F), each symbol indicates one mouse, and lines denote means. In (D), lines connect data from the same animal. * P<0.05; *** P<0.001; **** P<0.0001.

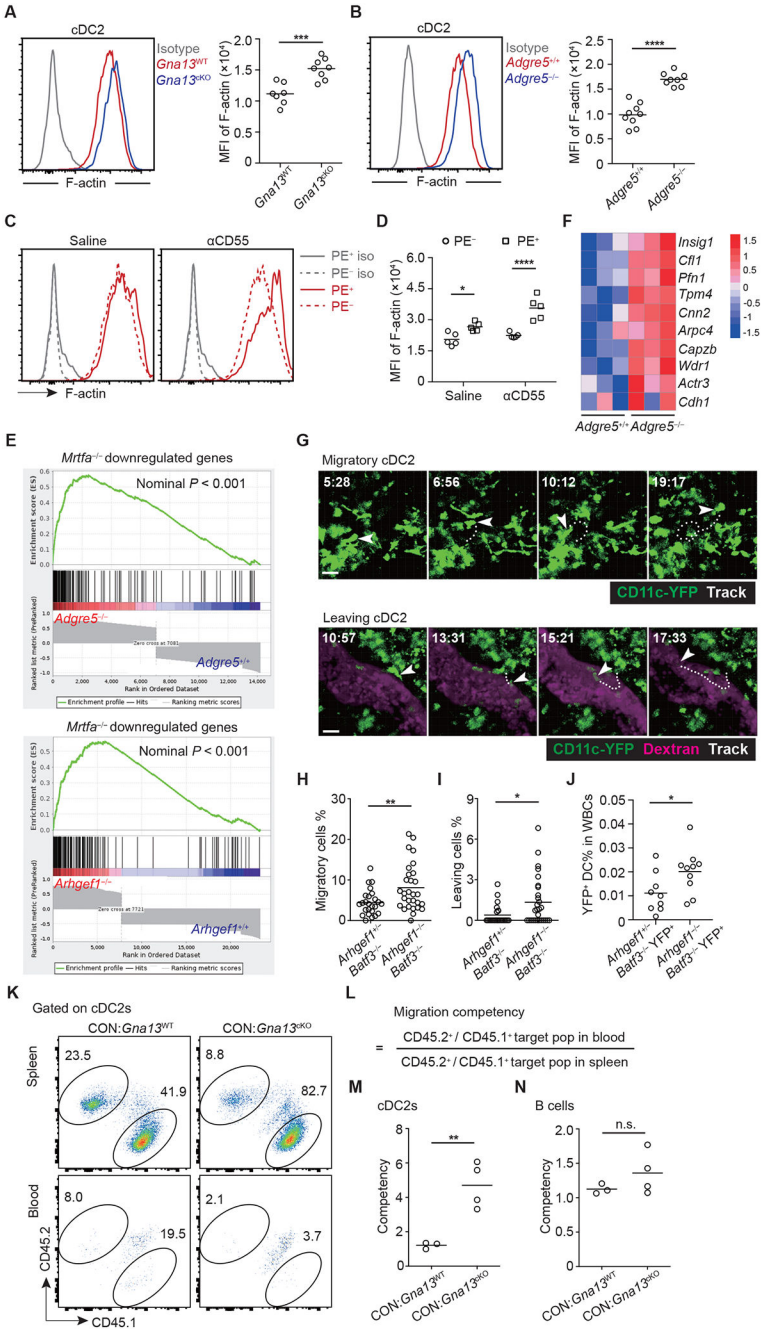

Fig. 5. CD97 pathway deficiency leads to increased F-actin and cDC2 motility.

(**A** and **B**) Representative (left) histogram and (right) MFI of F-actin in cDC2s from (A) *Gna13*^{cKO} or (B) *Adgre5*$^{-/-}$ and control mice. Data are pooled from two independent experiments. (**C** and **D**) Representative (C) histogram and (D) MFI of F-actin expression on in vivo PE labeled (PE^{+}) and PE non-labeled (PE^{-}) cDC2s in WT mice treated for 8 hours with antibody to CD55 or saline. Data are pooled from two independent experiments. (**E** and **F**) GSEA of *Mrtfa*$^{-/-}$ down-regulated genes compared with *Adgre5*$^{-/-}$ or *Arhgef1*$^{-/-}$ cDC2 dataset. (E) Enrichment profiles for genes that are down-regulated (P_{adj}< 0.001) in *Mrtfa*$^{-/-}$ BMDCs (29) compared with (top) *Adgre5*$^{-/-}$ and (bottom) *Arhgef1*$^{-/-}$ cDC2 datasets.

(F) Genes in the core enrichment, presented as a cluster-analyzed heatmap of expression levels of *Adgre5*$^{+/+}$ and *Adgre5*$^{-/-}$ cDC2 cells. (**G** to **I**) The motility of splenic cDC2 was observed with intravital two-photon microscopy in *Arhgef1*$^{+/-}$ *Batf3*$^{-/-}$ *Cd11c*-YFP and *Arhgef1*$^{-/-}$ *Batf3*$^{-/-}$ *Cd11c*-YFP chimeras. Dextran-TRITC was used to label large blood vessels. (G) Example of migratory cDC2 and leaving cDC2 (white arrowhead and dashed track, respectively) in *Arhgef1*$^{+/-}$ *Batf3*$^{-/-}$ *CD11c*-YFP or *Arhgef1*$^{-/-}$ *Batf3*$^{-/-}$ *CD11c*-YFP chimera spleen (movies S2 and S3). Time indicated in min:sec. Scale bar, 20 μm. (H) Frequencies of migratory cells (cDC2 with a minimum track length of 30 μm) in chimeras as indicated. (I) Frequencies of "leaving cells" (cDC2 that enter large vessels) in chimeras as indicated (movies S5 to S8). Each symbol indicates one movie in the supplementary materials. Lines denote the means. Data are pooled from five independent experiments. (**J**) Frequencies of YFP^{+} DCs in blood of *Arhgef1*$^{-/-}$ *Batf3*$^{-/-}$ and control chimeras. Data are pooled from two independent experiments. (**K** to **N**) Spleens from CD45.1 WT:CD45.2 *Gna13*^{cKO} or CD45.1 WT:CD45.2 *Gna13*^{WT} mixed chimeric mice were transplanted into CD45.1/2 WT recipients. The percentages of donor derived B cells and cDC2s from the recipient blood and transplanted spleens were examined 8 to 9 hours after surgery. (K) Representative flow cytometry profiles show gating strategies. (L) Equation for calculating the migration competencies of CD45.2^{+} population into blood. (M) Plots showing CD45.2^{+} competency values in individual chimera for cDC2s leaving spleen into blood. (N) Plots showing CD45.2^{+} competency values in individual chimera for B cells leaving spleen into blood. Data are pooled from three independent experiments. Each symbol indicates one mouse. Lines denote the means. * P<0.05; ** P<0.01; *** P<0.001; **** P<0.0001.

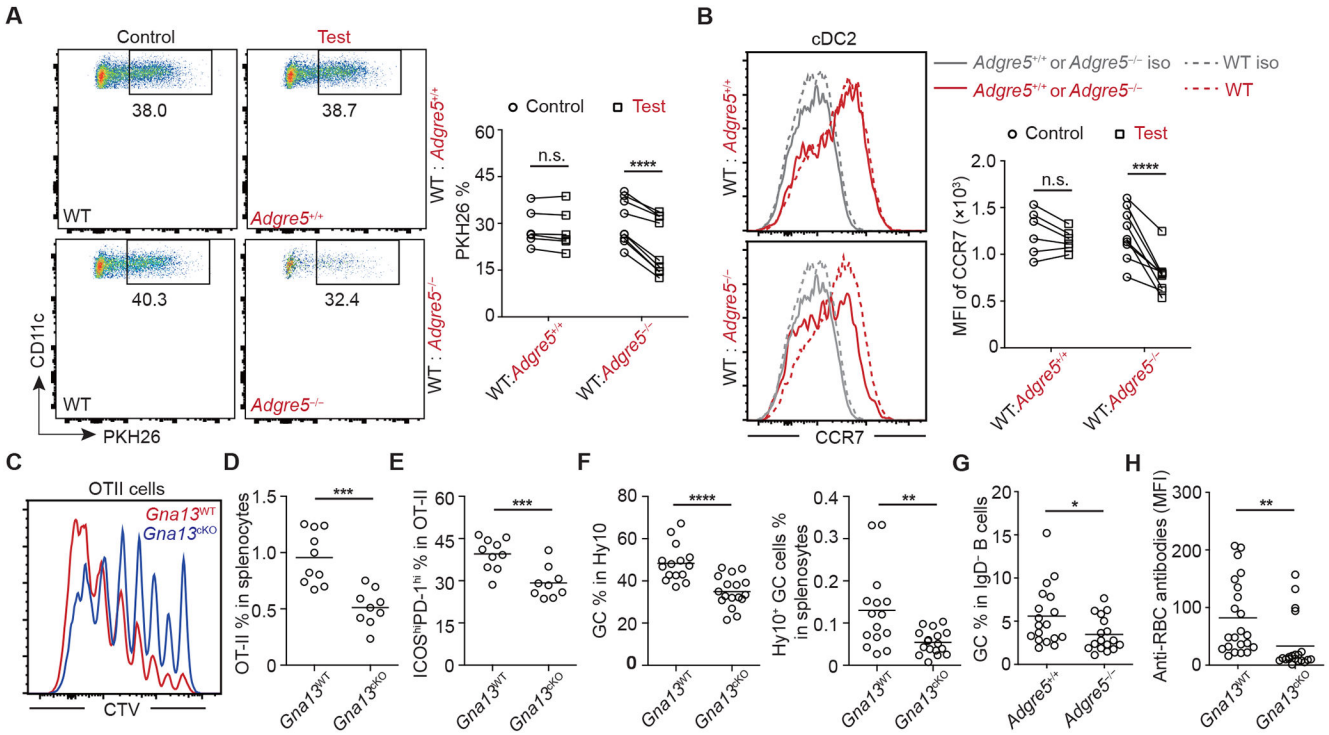

Fig. 6. Functional defects of CD97 pathway deficient splenic cDC2s.

(**A** and **B**) Mixed BM chimeras (WT: *Adgre5*$^{+/+}$ or WT: *Adgre5*$^{-/-}$) were analyzed 3 hours after PKH26-labeled SRBC injection. (A) Representative (left) flow cytometry plot and (right) frequencies of PKH26 dye-positive cDC2s. (B) Representative (left) histogram and (right) MFI of surface CCR7 expression on cDC2s from chimeras. (**C** to **E**) CellTrace Violet (CTV)-labeled OT-II T cells were transferred into *Gna13*^{cKO} and *Gna13*^{WT} mice. Mice were analyzed 3 days after SRBC-OVA immunization. [(C and D)] Representative (C) flow cytometry plot of proliferation and (D) frequencies of OT-II cells in total splenocytes. (E) Frequencies of ICOS^{hi}PD-1^{hi} T cells among transferred OT-II T cells. (**F**) Frequencies of GC B cells in (left) Hy10^{+} B cells and (right) frequencies of Hy10^{+} GC B cells in splenocytes in *Gna13*^{cKO} and control mice. (**G**) Frequencies of GC B cells in splenic IgD^{-}B220^{+} B cells in *Adgre5*$^{-/-}$ and control mice after HKLM immunization. (**H**) Antibodies to RBC in the sera of *Gna13*^{cKO} and control mice 3 weeks after transfusion of HEL-OVA-conjugated mouse RBCs. In (D) to (H), each symbol indicates one mouse, and lines denote means. Data are pooled from [(A to E)] two, (F) three, or [(G and H)] four independent experiments. In (A) and (B), lines connect data from same animal. * P<0.05; ** P<0.01; *** P<0.001; **** P<0.0001.

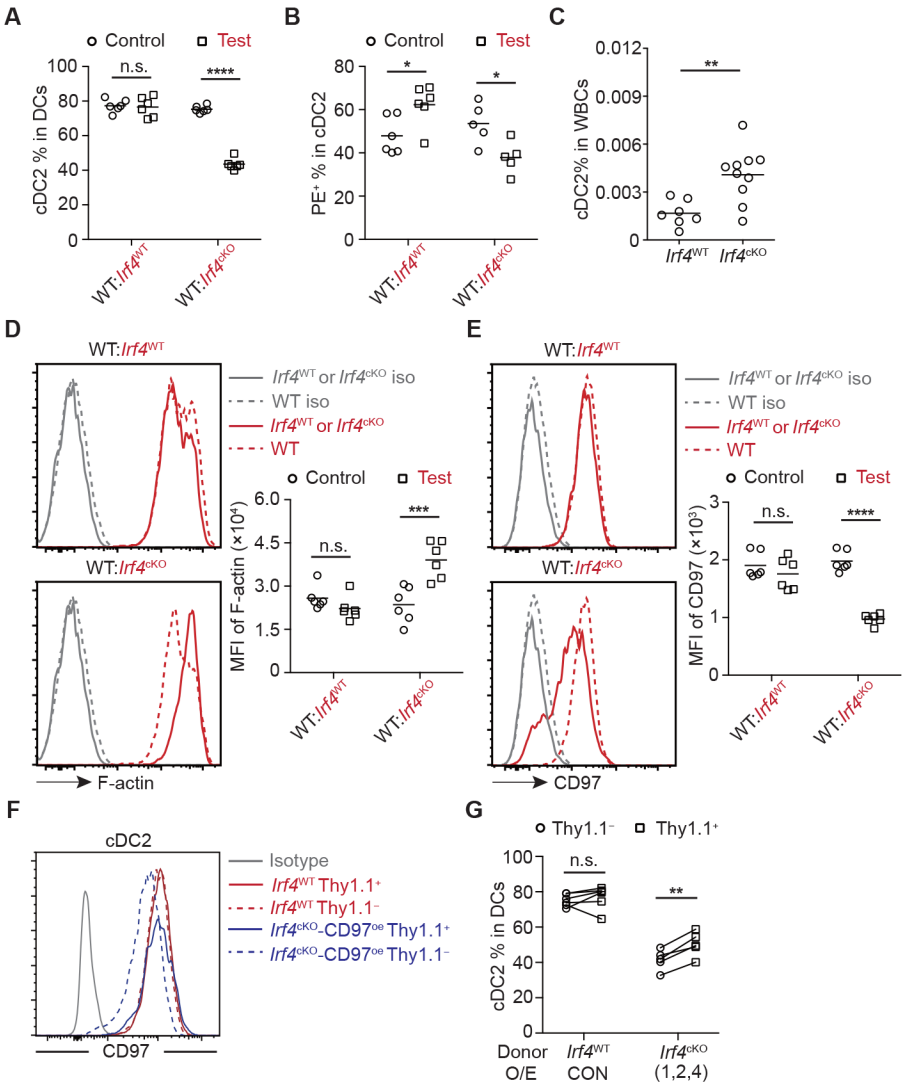

Fig. 7. CD97 action downstream of Irf4 in splenic cDC2s.

(**A** to **E**) Mixed (50:50) BM chimeras were made with CD45.1 WT (*Irf4*^{WT}) and CD45.2 *Irf4*^{WT} or *Cd11c*-cre *Irf4*$^{fl/fl}$ (labeled as *Irf4*^{cKO}) BM cells. [(A and B)] Frequencies of (A) cDC2s in DCs and (B) in vivo PE-labeled cells in cDC2s in each compartment of the indicated chimeras. (C) Frequencies of cDC2s in blood of *Irf4*^{cKO} and control mice. [(D and E)] Representative (left) histogram and (right) MFI of (D) F-actin expression and (E) surface CD97 expression on cDC2s in each compartment of the mixed chimeras. (**F** and **G**) BM chimeras were reconstituted with *Irf4*^{WT} or *Irf4*^{cKO} BM cells transduced with Adgre5 (1,2,4) or empty vector, with Thy1.1 as a reporter. (F) Representative histogram plots of surface CD97 on Thy1.1^{+} and Thy1.1^{-} cDC2s and (G) frequencies of cDC2s in Thy1.1^{+} or Thy1.1^{-} DCs of chimeras reconstituted as indicated. In (A) to (E), each symbol indicates one mouse, and lines denote means. In each summary graph, data are pooled from two independent experiments. In (G), lines connect data from same animal. * P<0.05; ** P<0.01; *** P<0.001; **** P<0.0001.